

## Nanosheets of Co-(Ni and Fe) Layered Double Hydroxides for Electrocatalytic Water Oxidation Reaction

Ricardo Valdez<sup>1,\*</sup>, Douglas B. Grotjahn<sup>2</sup>, Diane K. Smith<sup>2</sup>, Juan M. Quintana<sup>3</sup>, Amelia Olivas<sup>4</sup>

<sup>1</sup> PCellM, Centro de Nanociencias y Nanotecnología, UNAM, Km. 107 Carr. Tij-Ens, 22860, Ensenada, B.C. Mexico.

<sup>2</sup> San Diego State University, Department of Chemistry and Biochemistry, 5500 Campanile Drive, San Diego, California 92182-1030, United States.

<sup>3</sup> Facultad de Ciencias Químicas e Ing., UABC. Calz. Universidad No. 14418, Parque Industrial Internacional Tijuana, 22390 Tijuana, B.C. Mexico.

<sup>4</sup> Centro de Nanociencias y Nanotecnología, UNAM, Km. 107 Carr. Tij-Ens, 22860, Ensenada, B.C. Mexico.

\*E-mail: [rvaldez@cryn.unam.mx](mailto:rvaldez@cryn.unam.mx)

*Received:* 30 September 2014 / *Accepted:* 29 October 2014 / *Published:* 2 December 2014

---

The discovery of new nanomaterials as catalysts to produce hydrogen through artificial photosynthesis approach has become essential in the development of sustainable energy infrastructures. Large hydrogen demands could be tackled by splitting water into storable hydrogen and oxygen. Here, we report a novel nanomaterial that consists of a layered double hydroxide (LDH) based on Co-Fe and well-dispersed Co-Fe hydroxide nanoparticles (NPs) that is capable to perform the water oxidation reaction (WOR) effectively. Also, we compared the electrocatalytic behavior of this layered material against a Co-Ni LDH in WOR. Cyclic Voltammetry (CV) results show that the Co-Fe LDH catalyst exhibits lower overpotential (i.e., ~200 mV less, in aqueous 0.1 M phosphate buffer at neutral pH) than Co-Ni LDH. We attribute this behavior to a synergistic effect between the Co-Fe hydroxide NPs and Co-Fe LDH; different morphology of the Co-Fe hydroxide in contact could lead to a change in the electronic structure of the surface.

---

**Keywords:** Nanosheets, layered double hydroxide, oxygen evolution, water oxidation, cobalt-iron, nanoparticles

### 1. INTRODUCTION

The use of layered double hydroxides as efficient catalysts for WOR (half of water splitting) has attracted much attention in the last years [1–6]. The crystal structure of most of them corresponds

to that of a hydrotalcite, a natural magnesium–aluminum hydroxycarbonate, discovered in Sweden around 1842 [7]. LDHs have a generic formula as  $[M^{2+}_{(1-x)}M^{3+}_{(x)}(OH)_2]^{x+}(A^{n-})_{(x/n)} \cdot mH_2O$ , where  $M^{2+}$  and  $M^{3+}$  are divalent and trivalent cations occupying the octahedral positions within the hydroxide layers and  $A^{n-}$  the interlayer anions balancing the positive charges [8]. It is also important to develop efficient catalysts to obtain clean fuels, for example, splitting water into pure ( $H_2$  and  $O_2$ ) using the generous energy of sunlight for further use in replacement of conventional energy sources [9–11]. The water oxidation reaction ( $2H_2O \rightarrow O_2 + 4e^- + 4H^+$ ) is considerably more difficult than the hydrogen evolution reaction ( $4H^+ + 4e^- \rightarrow H_2$ ) half, because WOR requires a four-electron oxidation of two water molecules coupled to the removal of four protons to form a relative weak oxygen-oxygen bond [12]. Nowadays,  $RuO_2$  and  $IrO_2$  catalysts perform the WOR efficiently, but the use of these oxides at large scale will be difficult due to their high cost and limited availability [13–15]. Also, there has been an increasing interest in designing efficient catalysts containing plentiful materials, such as  $Co_3O_4$  [16, 17], and  $\alpha-Fe_2O_3$  [18]. In a recent study, an electrocatalyst for WOR based on Co–Ni LDH with impurities of  $Co(OH)_3$  showed a hexagonal platelet morphology [19]. However, to the best of our knowledge, a comparison of pure Co–(Ni and Fe) LDHs with well-defined morphology as nanosheets (NSs) has not been reported for electrocatalytic WOR. In this study, we show that Co–(Ni and Fe) LDHs with layered morphology are promising electrocatalyst to be used in WOR. Also, we show that a poorly crystalline material based on Co–Fe LDH which is decorated with Co–Fe hydroxide NPs performs the electrocatalytic WOR better than Co–Ni LDH in phosphate buffer at pH 7.

## 2. EXPERIMENTAL

### 2.1. Preparation of Co–Ni LDH.

In a general synthesis, 92 mL of ethanol were heated at 45 °C. Then, 952.6 mg of Cobalt (II) chloride hexahydrate ( $CoCl_2 \cdot 6H_2O$ , 99.1%) and 519.1 mg of nickel (II) chloride ( $NiCl_2 \cdot H_2O$ , 99.9%), each dissolved in 8 mL of mili-Q water (resistivity of 18.2  $M\Omega \cdot cm$ ), were added to the ethanol with magnetic stirring. The temperature of the solution was maintained at 45 °C for 10 min and then 20 mL of  $NH_3$  (with a concentration of 7N) was dropwise added under magnetic stirring. Finally, the temperature was increased and kept constant at 80 °C for 3 h with constant stirring. The precipitate was recovered by centrifuge at 3400 rpm at room temperature (RT). After centrifugation, the precipitate was washed twice with ultrapure water followed by once with acetone. Final pale-green product was dried overnight at high vacuum and then stored under  $N_2$  atmosphere.

### 2.2. Preparation of Co–Fe LDH decorated with Co–Fe hydroxide NPs

We followed a similar procedure as the Co–Ni LDH was prepared, with minor modifications. Usually, 46 mL of ethanol were heated at 45 °C. Then, 498.26 mg of  $Co(CH_3COO)_2 \cdot 4H_2O$  and 347.16 mg of  $Fe(CH_3COO)_2 \cdot 4H_2O$  (each dissolved in 4 mL of deionized water) were mixed with the ethanol. After that, the solution temperature was maintained at 45 °C for 10 min and then 10 mL of  $NH_3$  (with a

concentration of 7N) was dropwise added under magnetic stirring. Finally, the temperature was increased and kept constant at 80 °C for 3 h with constant stirring. The precipitate was recovered by centrifuge at 3400 rpm at RT. After centrifugation, the precipitate was washed once with acetone followed by twice with deionized water. Final brown product was dried overnight at high vacuum and then stored under N<sub>2</sub> atmosphere.

### 2.3. Physicochemical characterization.

The resulting compounds were characterized by low- and high- resolution transmission electron microscopy (TEM and HRTEM) and electron dispersive X-ray (EDX) using either a JEOL JEM–2100F or JEOL JEM–2010 electron microscope at 200 kV. X-ray diffraction measurements were performed with an X'Pert Phillips diffractometer, working at 45 kV and 40 mA, and using Cu K $\alpha$  radiation ( $\lambda = 1.5406 \text{ \AA}$ ), making a sweep in angles of  $2\theta$  from 5° to 65°, with a step size of 0.02. Nitrogen adsorption–desorption isotherms were collected at –196 °C, using a Micromeritics Tristar 3000 analyzer. Specific surface areas of the samples were measured by Brunauer-Emmett and Teller method. The metal loadings were determined by Inductively Coupled Plasma–Atomic Emission Spectroscopy (ICP-AES), with a Varian Liberty 110 equipment. FT-IR spectra were identified with a Perkin Elmer Spectrum 400 FT-IR/FT-NIR spectrometer from 600 to 4000 cm<sup>-1</sup>.

### 2.4. Electrochemical measurements.

All electrochemical data were collected on a CH Instrument model CHI760d digital potentiostat. Electrochemical experiments were performed in a three electrode configuration, using a glassy carbon electrode (GCE) as working electrode with a working area ( $S = 0.071 \text{ cm}^2$ ), a saturated calomel electrode (SCE) and a platinum wire as a counter electrode. Before electrochemical measurements, each GCE was polished with alumina (0.25–0.05  $\mu\text{m}$ , Buehler Ltd) on soft lapping pads and finally cleaned with water/acetone to remove any impurities. To prepare the working electrode, we followed a procedure reported elsewhere with minor modifications [2]. In brief, 0.5 mg of catalyst, 20  $\mu\text{L}$  of 5 wt. % Nafion solution and 3 mg of carbon black were dispersed in ethanol (180  $\mu\text{L}$ ) with sonication for at least 30 min to form a homogeneous mixture. Then, 1  $\mu\text{L}$  of this paste was drop-casted onto a GCE and left to dry in air at RT. A virtually identical mass loadings were used to achieve 0.035 mg·cm<sup>-2</sup> of catalyst in each electrochemical experiments. The carbon black was incorporated to create a more conductive material [20]. Finally, the prepared GCE was immersed in a 5 mL volume of 0.1 M phosphate buffer (KPi) under RT, at pH 7.0. The oxygen in solution was purged by bubbling N<sub>2</sub> for a minimum of 20 min before measurements.

## 3. RESULTS AND DISCUSSION

First, we identified the crystalline phases of the LDH compounds by powder X-ray diffraction (XRD) as shown in Figure 1. There were difficulties in analyzing the results trying to identified the

crystallographic structure of LDHs, since disorder may be present in the stacking of the layers, lowering the symmetry and giving rise to considerable differences in relative intensities [8]. However, the XRD pattern of the Co-Ni based material can be indexed as a rhombohedral Co-Ni LDH (JCPDS card No. 33-0429) without other phase traces. The XRD pattern of Co-Ni LDH is in accordance with a similar compound reported in the literature [21]. In the same figure, the results of XRD showed a poorly crystalline Co-Fe based material that was identified as Co-Fe LDH, and also with a rhombohedral structure (JCPDS card No. 50-0235). As it is well known, frequently the amorphous materials are able to present a great catalytic activity and these results are showing us poorly crystalline materials, but with evident phases and no other compounds were detectable by this technique.

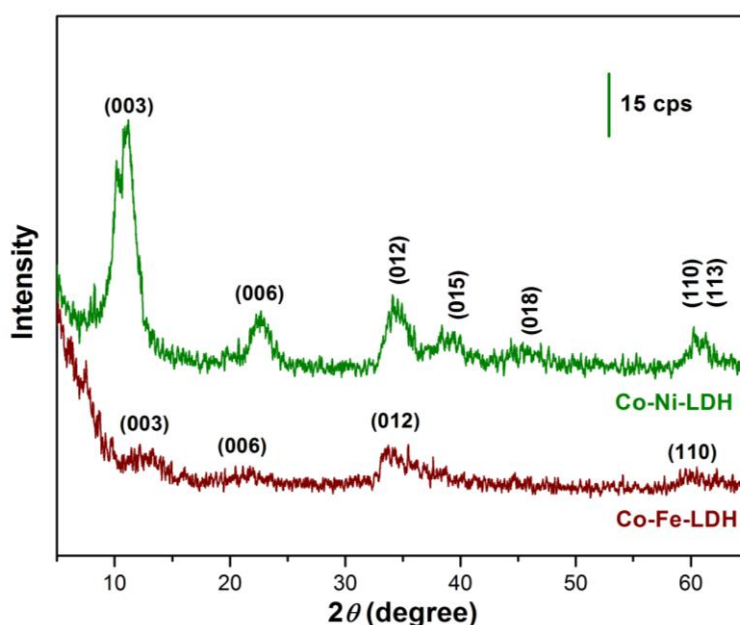


**Figure 1.** X-ray diffraction patterns corresponding to Co-Ni LDH and Co-Fe LDH.

Second, we identified the  $A^{n-}$  in the LDH interlayers by Fourier transform infrared spectroscopy (FT-IR). In natural hydrotalcite these interlayer anions are carbonate and water molecules [7].  $(CO_3)^{2-}$  ions may arise from possible slight dissolution of  $CO_2$  from air [19]. In the FT-IR spectrum of Co-Ni LDH is observed a wide band at  $3418\text{ cm}^{-1}$  assigned to O-H stretching from  $H_2O$ . Moreover, the band at  $1628\text{ cm}^{-1}$  is attributed to H-O-H from deformation of water. At  $1365\text{ cm}^{-1}$  appears a band caused by the carbonate ions, and the two bands on  $1100\text{ cm}^{-1}$  and  $890\text{ cm}^{-1}$  are consistent with a deformation of  $H_2O$  or  $OH^-$ . Finally, the band at  $650\text{ cm}^{-1}$  is consistent with the vibration of cation-oxygen [22]. On the other hand, the FT-IR spectrum of Co-Fe LDH also in Figure 2 (red-wine color) showed a wide band at  $3325\text{ cm}^{-1}$  assigned to O-H stretching, other bands at  $1546$ ,  $1410$  and  $1343\text{ cm}^{-1}$  are agreeing to acetate [23]. The bands at  $1546$  and  $1410\text{ cm}^{-1}$  have been ascribed to the asymmetric and symmetric stretching of the carboxylate group ( $-CO_2^-$ ), respectively, whereas the band at  $1343\text{ cm}^{-1}$  corresponds to symmetric C-H bending of methyl group,  $\delta_s(CH_3)$  [24]. In this

case, the carbonate ions are not obvious in the Co-Fe LDH spectrum, likely because the band is hidden between the 1343 and 1410  $\text{cm}^{-1}$  bands.

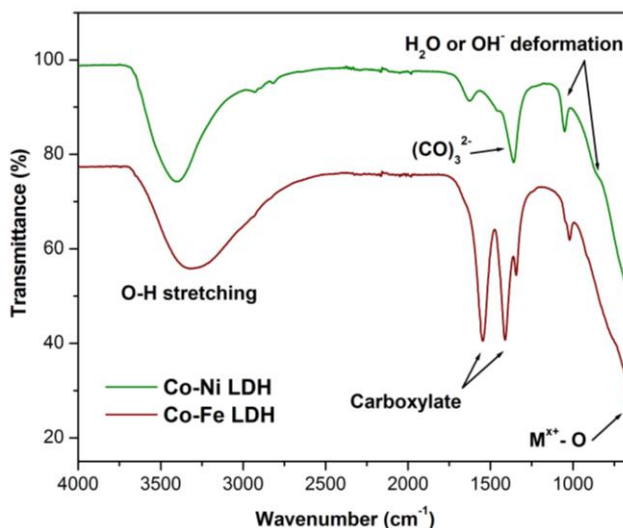


**Figure 2.** FT-IR spectra corresponding to Co-Fe LDH and Co-Ni LDH compounds.

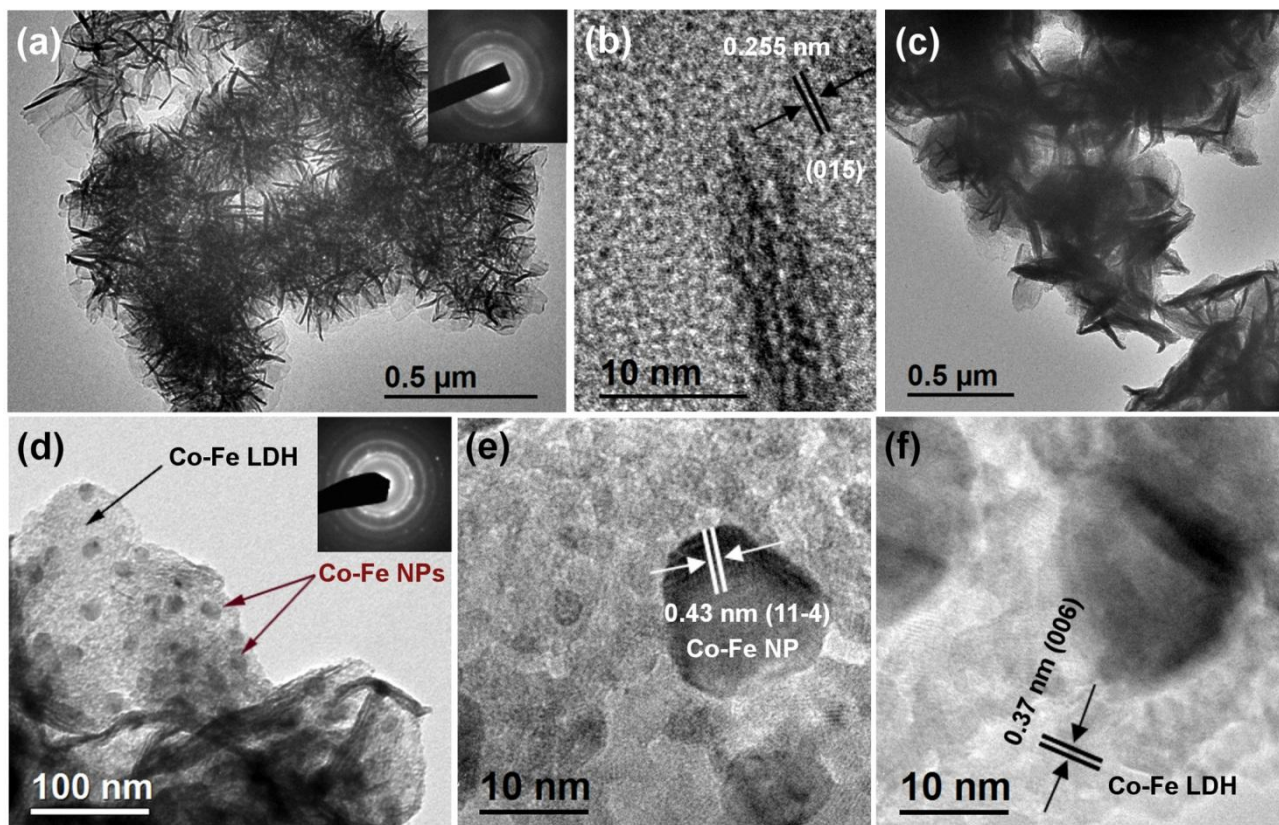


**Figure 3.** (a) Bright-field TEM micrograph of Co-Ni LDH; inset (SAED). (b) HRTEM micrograph of Co-Ni based material. (c) Bright-field TEM micrograph of Co-Fe LDH. (d) HRTEM micrograph of Co-Fe LDH, inset (SAED). (e) HRTEM micrograph of Co-Fe LDH that it is showing the lattice fringe of the NPs. (f) HRTEM micrograph of Co-Fe LDH that it is showing the lattice fringe of LDH morphology.

By examining different regions of the Co–Ni LDH by TEM, nanosheets of ~300 nm in length with well-defined morphology were observed as shown in Figure 3a. The selected area electron diffraction (SAED) showed in the inset confirmed the material crystallinity. Furthermore, HRTEM results shows a lattice fringe of 0.225 nm, corresponding to the (015) plane in the Co–Ni LDH material (Figure 3b). Also, the Co–Fe based material was identified as a layered material with NSs of size about ~0.5  $\mu\text{m}$  (Figure 3c). More importantly, Co–Fe LDH showed a layered structure decorated with well-dispersed NPs as is observed in Figure 3d. The Co–Fe layered material shows a fringe lattice of 0.37 nm (006) on the NSs confirming the rhombohedral phase as well as determined by XRD (Figure 3e), and the dispersed NPs present an interplanar distance of 0.43 nm (11–4) corresponding to the  $\text{Co}(\text{OH})_2 \cdot \text{Fe}(\text{OH})_3 \cdot 5\text{H}_2\text{O}$  monoclinic phase (JCPDS card No. 55-0124) as shown in Figure 3f. In fact, the Co–Fe hydroxides NPs were not detected by XRD measurements, due to low intensity of the peaks in the XRD pattern of Co–Fe LDH. In addition, we determined the ratio of metals in the bulk by ICP-AES that were found to be (Co/Ni, 3:1) for Co–Ni LDH and (Co/Fe, 0.7:1) for Co–Fe LDH.

To gain information on the catalytic performance of the prepared NSs, we carried out an electrochemical experiment where pure oxygen and air were separately added to a solution containing 1.2 mg of the as-prepared Co–Ni LDH (previously dispersed in 5 mL of phosphate buffer at pH 7 with sonication by ~10 min). The results showed two oxidation events that correspond to  $\text{Co}^{2+/3+}$  and  $\text{Co}^{3+/4+}$  redox steps [25, 26], and another more that coincides with catalytic WOR. Moreover, the production of  $\text{O}_2$  is confirmed by the observation of a reduction peak on the return at scan at  $-0.6$  V vs NHE, whose intensity increases upon addition of air or pure  $\text{O}_2$  to the solution (Figure 4). In addition, we monitored each run with a portable optical microscope and it was possible to see bubble formation at the overpotential.

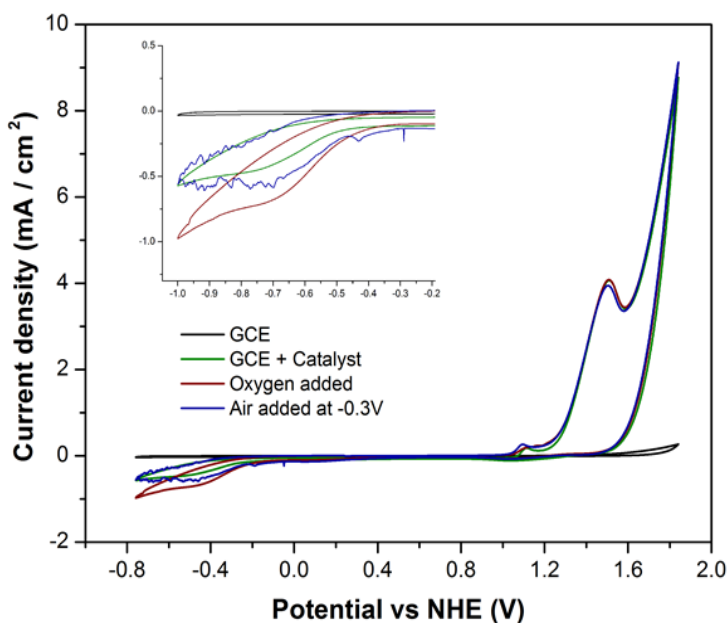


**Figure 4.** CV's of 1.2 mg of Co–Ni LDH catalyst dispersed in the phosphate buffer at a scan rate of  $100 \text{ mV} \cdot \text{s}^{-1}$ .

Subsequently, to evaluate the electrocatalytic behavior of our LDHs under similar experimental conditions, we prepared a carbon paste electrode containing the catalyst to immobilize the samples on the working electrode surface. Figure 5a shows the cyclic voltammograms (CV's) of the Co-(Ni and Fe) LDH catalyst-containing carbon paste electrodes. The CV of Co-Ni LDH exhibits two oxidation events at potentials (E) of 0.99 V and 1.47 V vs NHE before the catalytic wave, which correlate to the  $\text{Co}^{2+/3+}$  and  $\text{Co}^{3+/4+}$  redox steps [25, 26]. Then, a large catalytic current arises with an onset potential of 1.59 V, that is due to WOR. The CV of Co-Fe LDH shows an oxidation event at 1.32 V, corresponding presumably to the  $\text{Co}^{3+}$  to  $\text{Co}^{4+}$  redox processes [26]. Surprisingly, onset of the WOR occurs at 1.38 V. The Co-Ni LDH catalyst gave a current density (a measure of catalytic activity) of  $14.8 \text{ mA}\cdot\text{cm}^{-2}$  at 1.84 V in neutral pH, but at 1.64 V the current was about  $5 \text{ mA}\cdot\text{cm}^{-2}$ , but the catalytic current of Co-Fe LDH gives  $6.5 \text{ mA}\cdot\text{cm}^{-2}$  at 1.64 V and the onset for WOR is at 1.37 V, that is, a lower overpotential of  $\sim 200 \text{ mV}$  than the analogous Co-Ni catalyst as one can observe in the same figure. That means that Co-Fe LDH needs lower energy than Co-Ni LDH to perform the WOR efficiently. Note that for clear discussion and comparison with other reported catalysts, potentials (E) are converted to the NHE by using  $E(\text{NHE}) = E(\text{Hg}/\text{Hg}_2\text{Cl}_2, \text{sat. KCl}) + 0.241 \text{ V}$  [27]. Also, all current densities are reported per geometric area of working electrode. On the other hand, overpotentials were calculated following the equation:  $\eta = E(\text{appl}) - E(\text{O}_2/\text{H}_2\text{O})$  since;  $E(\text{appl})$  it is the potential from experimental water oxidation at onset and  $E(\text{O}_2/\text{H}_2\text{O})$  is the theoretical potential by oxygen evolving from water at pH 7 (810 mV vs NHE), coming from  $E_{\text{NHE}} = 1,230 \text{ mV}$  at pH = 0, and taking in account that the potential to produce oxygen decreases  $\sim 60 \text{ mV} \times \text{pH unit}$  [28].

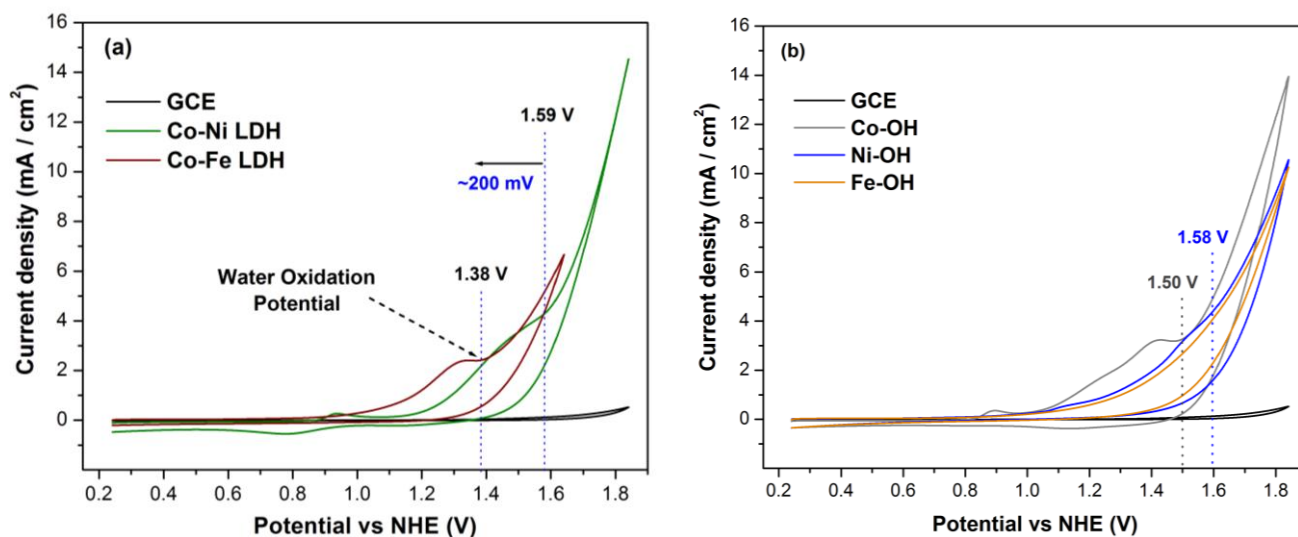


**Figure 5.** (a) Cyclic voltammograms of Co-Ni LDH and Co-Fe LDH catalysts with  $0.035 \text{ mg}\cdot\text{cm}^{-2}$  catalyst loading, recorded in 0.1 M phosphate buffer at pH 7.0. The black line corresponds to the glassy carbon electrode (GCE) without catalyst. (b) Comparison of the CV's of Co-OH, Ni-OH and Fe-OH synthesized under similar conditions as Co-(Ni and Fe) LDHs. All electrochemical experiments using carbon paste electrodes containing the catalyst were recorded at a sweep rate of  $20 \text{ mV}\cdot\text{s}^{-1}$ .

In addition to the electrocatalytic measurements, three more materials were synthesized under similar conditions as reference by using only Co, Ni or Fe as precursors. In Figure 5b, the CV of Co-OH shows an onset potential for O<sub>2</sub> evolution was *ca.* 1.5 V (i.e., an overpotential of ~690 mV), which is lower than those of Ni-OH and Fe-OH, whose overpotentials were found to be  $\eta \approx 770$  mV and  $\eta \approx 780$  mV, respectively. In conclusion, the overpotential toward water oxidation of the Co-containing materials increased in the order Co–Ni LDH  $\ll$  Co-OH  $\ll$  Co–Fe LDH. Furthermore, the trend in the catalytic current also favors to the Co–Fe LDH. For example, at 1.6 V, the current densities of Co–Ni LDH, Co-OH, and Co–Fe LDH were 4.39, 4.88 and 5.14 mA·cm<sup>-2</sup>, respectively. Hence, the current density of Co–Fe LDH is higher than those of Co-OH and Co–Ni LDH. We can see that the incorporation of nickel in the cobalt catalyst did not show a favorable behavior toward water oxidation. In contrast, the iron addition to the cobalt catalyst arise an enhancement in WOR performance, due to the high disorder on the structure caused by the Co-Fe hydroxide NPs. To compare the catalytic performance of our best catalyst (Co–Fe LDH) against the catalysts reported in literature, we found that the best catalysts based on Co<sub>3</sub>O<sub>4</sub> NPs (3 nm) proposed by Grzelczak *et al.* [17], it is showing an onset at 1.45 V (~640 mV) that is due to water oxidation. In the context of available cobalt catalysts, our catalyst exhibits overpotential of ~70 mV lower than the Co<sub>3</sub>O<sub>4</sub> NPs (3 nm) catalyst. However, direct comparison with results from other research groups is rather difficult since there are different experimental conditions. Although, we focused on the comparison of LDH nanosheets as promising catalysts for WOR, because NPs might be immobilized into the LDHs to produce a more active catalyst; it is known that a synergistic effect between a metal nanocatalyst and a LDH support can effectively promote further enhancement of catalytic activity [29]. The layered morphology that present those kind of materials, make more accessible the Co active sites and improve the fast diffusion of reactants/products (see scheme of the kind of structure in Figure 6).

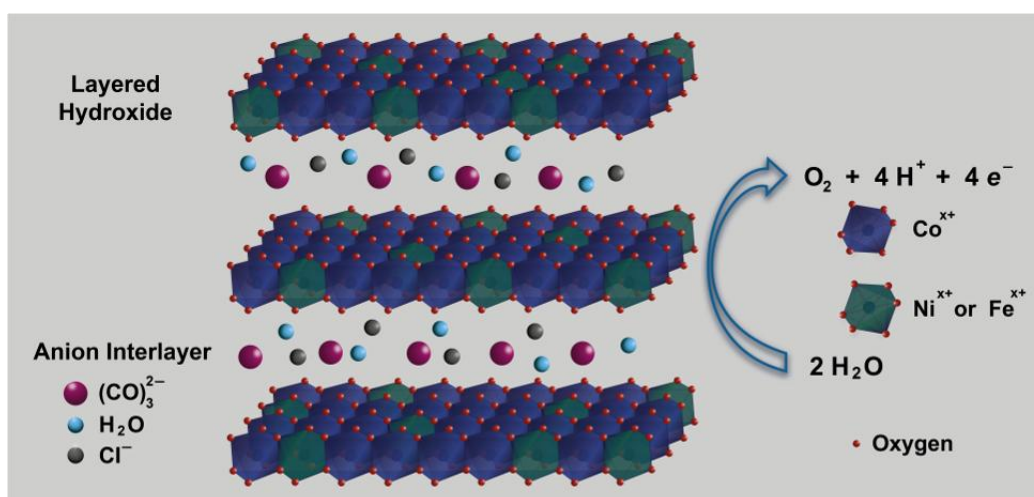


**Figure 6.** Scheme of the structure type that form the prepared LDHs in this study.

Moreover, the trend in the catalytic activity of the materials could be correlated with the materials' surface areas, as the BET surface area of Co–Ni LDH is 103 m<sup>2</sup>·g<sup>-1</sup> and that of Co–Fe LDH

is  $191 \text{ m}^2 \cdot \text{g}^{-1}$ . It is noteworthy to mention that the surface area values of our prepared compounds are higher than the other BET surface area values of LDHs reported for the WOR [2, 3]. A synergistic effect between Co–Fe hydroxide NPs and Co–Fe LDH enhanced electrocatalytic activity toward water oxidation (Figure 3d). We attribute the higher activity in WOR to morphological, structural and electronic properties of the Co–Fe LDH nanosheets as electrocatalyst. The highly dispersed iron possibly influences a change in the electronic properties of the Co–Fe LDH catalyst. These could be due to the electrons from iron or cobalt of the NPs are interacting with the electrons of the Co–Fe LDH surface, decreasing the overpotential for WOR.

#### 4. CONCLUSIONS

In the present study we show a reasonably facile synthesis to produce Co-(Ni and Fe) LDH with a layered morphology. Also, we are presenting a novel nanomaterial based on double layered hydroxides that is decorated with well-dispersed hydroxide NPs which one is able to perform the water oxidation reaction. The comparatively high surface area of these compounds could be used to immobilize other NPs known to be active for WOR, with the goal of reducing the overpotential of those materials. Cyclic voltammetry results showed that Co–Fe LDH is the most active electrocatalyst in our prepared materials for WOR. Moreover, the catalysts could be produced on large scale, since they are synthesized using inexpensive precursors under mild conditions.

#### ACKNOWLEDGMENTS

The authors would like to thank to F. Ruiz, E. Aparicio, M. Vega, E. Flores, I. Gradilla, J. Mendoza and J. J. Castro for their invaluable technical support. R. Valdez acknowledges a scholarship provided by Conacyt. This work was financed by PAPIIT 108613 and Conacyt 174492 grants.

#### References

1. G. Abellán, J. A. Carrasco, E. Coronado, J. Romero, M. Varela, *J. Mater. Chem. C.*, 2 (2014) 3723.
2. X. Zou, A. Goswami, T. Asefa, *J. Am. Chem. Soc.*, 135 (2013) 17242.
3. S. J. Kim, Y. Lee, D. K. Lee, J. W. Lee, J. K. Kang, *J. Mater. Chem. A*, 2 (2014) 4136.
4. B. Li, Y. Zhao, S. Zhang, W. Gao, M. Wei, *ACS Appl. Mater. Interfaces*, 5 (2013) 10233.
5. D. Tang, J. Liu, X. Wu, R. Liu, X. Han, Y. Han, H. Huang, Y. Liu, Z. Kang, *ACS Appl. Mater. Interfaces*, 6 (2014) 7918.
6. B. M. Hunter, J. D. Blakemore, M. Deimund, H. B. Gray, J. R. Winkler, A. M. Mueller, *J. Am. Chem. Soc.*, 136 (2014) 13118.
7. V. Rives, M. A. Ulibarri, *Coord. Chem. Rev.*, 181 (1999) 61.
8. F. Cavani, F. Trifirò, A. Vaccari, *Catal. Today*, 11 (1991) 173.
9. J. K. Hurst, *Science*, 328 (2010) 315.
10. S. Fukuzumi, Y. Yamada, *ChemSusChem*, 6 (2013) 1834.
11. N. Mirbagheri, D. Wang, C. Peng, J. Wang, Q. Huang, C. Fan, E. E. Ferapontova, *ACS Catal.*, 4 (2014) 2006.
12. W. K. Matthew, D. G. Nocera, *Science*, 321 (2008) 1072.
13. P. G. Hoertz, Y. I. Kim, W. J. Youngblood, T. E. Mallouk, *J. Phys. Chem. B*, 111 (2007) 6845.

14. Y. Zhang, E. C. Judkins, D. R. McMillin, D. Mehta, T. Ren, *ACS Catal.*, 3 (2013) 2474.
15. T. Nakagawa, C. A. Beasley, R. W. Murray, *J. Phys. Chem. C.*, 113 (2009) 12958.
16. J. Feng, F. Heinz, *Angew. Chem. Int. Ed.*, 48 (2009) 1841.
17. M. Grzelczak, J. Zhang, J. Pfrommer, J. Hartmann, M. Driess, M. Antonietti, *ACS Catal.*, 3 (2013) 383.
18. R. D. L. Smith, M. S. Prévot, R. D. Fagan, Z. Zhang, P. A. Sedach, J. M. K. Siu, S. Trudel, C. P. Berlinguette, *Science*, 340 (2013) 60.
19. Y. Zhang, B. Cui, C. Zhao, H. Lin, J. Li, *Phys. Chem. Chem. Phys.*, 15 (2013) 7363.
20. T. Grygar, F. Marken, U. Schröder, F. Scholz, *Collect. Czech. Chem. Commun.*, 67 (2002) 163.
21. H. Chen, L. Hu, M. Chen, Y. Yan, L. Wu, *Adv. Funct. Mater.*, 24 (2014) 934.
22. P. Piret, M. Deliens, *Bull. Mineral.*, 103 (1980) 113.
23. J. M. Delgado, A. Rodes, J. M. Orts, *J. Phys. Chem. C.*, 111 (2007) 14476.
24. G. Socrates, *Infrared and Raman Characteristic Group Frequencies*, John Wiley & Sons, Chichester, U.K., (2001).
25. N. H. Chou, P. N. Ross, A. T. Bell, T. D. Tilley, *ChemSusChem*, 4 (2011) 1566.
26. J. B. Gerken, J. G. McAlphin, J. Y. C. Chen, R. D. Britt, S. S. Stahl, *J. Am. Chem. Soc.*, 133 (2011) 14431.
27. A. J. Bard, L. R. Faulkner, *Electrochemical Methods, Fundamentals and Applications*, 2ed. John Wiley & Sons, (2001).
28. L. Tong, A. Iwase, A. Nattestad, U. Bach, M. Weidener, G. Gotz, A. Mishra, P. Bauerle, R. Amal, G. G. Wallace, A. J. Mozer, *Energy Environ. Sci.*, 5 (2012) 9472.
29. S. He, Z. An, M. Wei, D. G. Evans, X. Duan, *Chem. Commun.*, 49 (2013) 5912.

© 2015 The Authors. Published by ESG ([www.electrochemsci.org](http://www.electrochemsci.org)). This article is an open access article distributed under the terms and conditions of the Creative Commons Attribution license (<http://creativecommons.org/licenses/by/4.0/>).